Normalized roughness length estimation using derived sea state parameters from SAR

Abdalmenem Owda[(1)], Andrey Pleskachevsky[(2)], Merete Badger[(1)], Xiaoli Guo Larsén[(1)] , Dalibor Cavar[(1)]

(1) Technical University of Denmark, Department of Wind and Energy Systems, Frederiksborgvej 399, Roskilde, Denmark

(2) German Aerospace Center (DLR), Maritime Safety and Security Lab Bremen, Am Fallturm 9, 2. OG Bremen, Germany

ABSTRACT

Studying air-sea interaction is essential for various coastal applications and structures, including offshore wind energy. The impact of waves on the atmospheric models is often described by introducing of the aerodynamic roughness length (z_0) parameter, which is derived from various wave-related parameters. The global coverage and free-accessibility of Synthetic Aperture Radar (SAR) have the potential to enhance the coupling of atmosphere and wave using Sentinel 1-interferometric wide mode (S1-IW) in areas up to a few kilometers from coasts. This study introduces a method to overcome the so-called cutoff effect by imaging of sea state shorter than approximately 120 m using S1-IW. The validation of derived wave parameters from S1-IW against reference measurements was performed to assess the reliability of SAR images in wave related applications. The root- mean square error (RMSE) of derived significant wave height (H_s) and second moment wave period (T_{m2}) using the CWAVE_EX algorithm were 0.43 m and 0.8 sec, respectively. Significant reductions in H_s and peak wavelengths (L_p) were observed in shallow water depths. The z_0 was estimated using the well-known roughness scheme "*Taylor and Yelland*" and normalized for several positions in the study area. Significant differences in z_0 between shallow and deep waters for offshore winds (winds coming from land). Most buoys located at water depths and distances to the coastline less than 50 m and 50 km, respectively exhibited high values of z_0.

Keywords— Roughness length, SAR, significant wave height, spectral peak wavelength, JONSWAP, bathymetry.

1. INTRODUCTION

The interaction between the atmosphere and the ocean, through ocean surface waves, has a significant impact on the transfer of momentum and heat across the atmospheric boundary layer. Conventionally, the roughness length (z_0), which defines the height where the wind speed theoretically is zero in the empirical stable vertical log-profile. z_0 is commonly used in most atmospheric and ocean models as a function of the friction velocity (u_*), the acceleration due to gravity (g), and Charnock's coefficient (α_{ch}), $z_0 = \frac{\alpha_{ch} u_*^2}{g}$, where u_* and α_{ch} are impacted by the sea state [1] . z_0 is one of the key parameters for describing and characterizing the marine atmospheric boundary layer (MABL) [2] and the study of air-sea interaction. Accurate estimation of the wind energy production for offshore wind turbines depends to a high degree on accurate estimation of z_0, which is used to extrapolate the wind speed up to turbines' hub height. Using constant value for z_0 can lead to significant errors (in many applications for open calm ocean $z_0 = 0.0002$ m).

[3] argues that the z_0 appears to differ between deep and shallow waters. In shallow waters the sea-surface waves are modulated by many complicated mechanisms, refraction by bathymetry being one of these mechanisms.

Obtaining a representation for z_0 is still a debated issue. Various schemes have been introduced using the sea-state parameters such as wave age, peak wavelength (L_p), wave steepness and significant wave height (H_s) [4]. [5] proposed that the z_0 can be predicted from the height and steepness of the waves based on the ratio between the H_s and the L_p.

Synthetic Aperture Radar (SAR) on space born satellites are active microwave systems that operate nearly independently of weather conditions, day-and-night, and cloud coverage. SAR imagining is particularly suitable for coastal applications, thanks to its high spatial resolution and global coverage. Europe's Copernicus program by the European Space Agency (ESA) is one of most ambitious programs and provides free access to all Sentinel mission data including Sentinel-1A/B SAR data (https://scihub.copernicus.eu/).

[6] introduced a method for estimating a series of sea state parameters from different SAR satellites and modes. The CWAVE_EX algorithm estimates the total H_s (m), dominant $H_s^{swell-1}$ (m) and secondary swell wave $H_s^{swell-2}$ (m), windsea wave height H_s^{wind} (m), the mean wave period T_{m0} (sec) the first T_{m1}(sec), the second moment wave period T_{m2} (sec) and wind sea period T^{wind}.

The main goal of this study is to estimate the variation on z_0 within a coastal area. The east coast of the United States has been taken as the validation area. We quantify the differences in normalized z_0 between open ocean and shallow waters. Using SAR data, which provides global coverage in quantifying roughness length, will enhance using its derived wave parameters in the coupling of atmosphere and wave models. The study area, data and method are presented in Section 2. Results are demonstrated in Section 3. Finally, a discussion and main conclusion are recapped in Section 4.

2. DATA, STUDY AREA AND METHOD

2.1. Data

2.1.1. SAR-IW data

Sentinel-1 (S1) A/B is a C-band (5.405 GHz) constellation of two satellites orbiting the Earth at altitude 704 km with a 6-day repeat cycle. Sentinel-1A (2014-now) and Sentinel-1B

(2016-2021) provide four different acquisition modes and support operation in single (HH or VV) or dual (HH+HV or VV+VH) polarization. In this study, interferometric wide (IW) swath mode was chosen due to the abundance of this type of data in coastal regions. Ground range detected high resolution (GRDH) resolution products- level 1, with 10 × 10 m pixel spacing and VV polarization, were processed.

2.1.2. In situ measurements

Ocean buoy observations - National Data Buoy Center (NDBC), from the US National Oceanic and Atmospheric Administration (NOAA) were used to validate against the computed H_s and T_{m2} retrieved from the SAR-IW data. Optimized L_p is compared with the computed L_p using dominant wave period (DPD), denoted as (L_{p-DPD}). Twenty buoys were found to be collocated spatially within SAR scenes and positioned closer than 3 km to the image borders. The shorter collocated distance is used because of high sea state variability in coastal regions.

2.2. Study area

The east coast of the United States is chosen for this study. It has SAR coverage from 2014-2022 and Twenty NDBC buoys. The buoys are distributed along the coastline at different water depths and distances to the coastline as illustrated in Fig. 1.

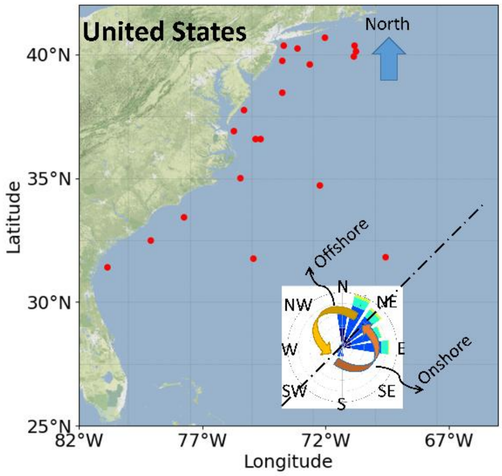

Fig.1. The study area along the east coast of the United States. Red dots refer to the 20 NDBC buoys used for sea state parameter validation. The wind rose refers to the wind direction for collocated SAR scenes (obtained from the global forecasting system model). The wind sectors for offshore (0°-45°, 360°-225°) and onshore (45°-225°) are illustrated.

2.3. Methods

2.3.1. Retrieval of sea state parameters from SAR-IW

The CWAVE_EX (Extended CWAVE) algorithm has a series of data preparation steps consisting of SAR scene reading, calibration, land masking, subscene preparation, image outlier filtering, smoothing and de-noising depending on the SAR mode used. Additionally, the SAR signal from the ocean waves is frequently distorted by a series of artefacts (e.g., ships, ship wakes, oil spills, etc.). All these distortions and conditions result in a very noisy SAR image spectrum where wave-generated peaks are undiscernible. The image spectrum analysis is, therefore, complemented by a series of additional steps including texture analysis, e.g., grey level co-occurrence matrix. Eight integrated sea state parameters can be derived (H_s , T_{m0} , T_{m1} , T_{m2}, T^{wind} , $H_s^{Swell-1}$, $H_s^{Swell-2}$, H_s^{wind})[7]. Among these derived parameters, only H_s and T_{m2} were validated against the corresponding NDBC measurements. As data validity control of the remote sensing data, additional filters were introduced for H_s and T_{m2}. Only H_s larger than 0.10 m and T_{m2} larger than 2 sec were considered.

There are also some limitations for using S1 C-band imagery. The coarse IW image resolution and high satellite altitude impose a limit for mapping on moving targets. Therefore, only long wavelengths can be clearly mapped in S1-IW images, due to the cutoff effect by imagining sea state of shorter waves than 120 m. This means, the peak direction and L_p cannot be directly estimated from SAR image spectrum. Notably, for z_0 estimation, the most important parameters are the H_s and the L_p.

2.3.2. Peak wavelength esimation using JONSWAP and Dispersion

To obtain the peak frequency (fp), the JONSWAP spectrum model has been applied by optimization of the sea state parameters integrated from JONSWAP and estimated from S1-IW imagery. The JONSWAP model [8] was considered on range of frequencies from 0 Hz to 1 Hz and for series of fetch distances ranging from 20 km to 150 km. For participation in the spectrum for swell and wind sea parts, the threshold of 0.125 Hz (corresponds to 8 sec period) was applied based on local measurements statistics. The statistical n-order momentum of the spectrum in frequency domain can be obtained by numerical integration of the energy over the wave spectrum as

$$m_n = \int_{f=0}^{f=1} S(f) f^n \, df, \qquad (1)$$

where $S(f)$ is the wave spectral density of JONSWAP in the frequency domain, f is the frequency range of the waves between 0 Hz and 1 Hz. The following sea state parameters were computed as illustrated in the following equations:

$$H_s = 4\sqrt{m_0}, H_s^{swell} = 4\sqrt{m_{0,swell}}, H_s^{wind} = 4\sqrt{m_{0,wind}}, T_m = \frac{m_{-1}}{m_0}, T_{m1} = \frac{m_{-1}}{m_0}, T_{m2} = \sqrt[2]{\frac{m_0}{m_2}}. \qquad (2)$$

The peak frequency was estimated by minimization of an error by:

$$\sigma = \sqrt{\sum_{i=0}^{i=n} (\sigma_i)^2} \longrightarrow 0, \qquad (3)$$

where σ_i means absolute error of an integrated sea state parameter estimated form JONSWAP and S1-IW imagery, i means the parameter number, e.g., for i =1, $\sigma_1 = H_s^{JONSWAP} - H_s^{S1-IW}$, and n is the number of parameters (n=6).

sea state parameters include two swell components - namely the dominant and the secondary systems. As JONSWAP cannot separate these two components, as the total swell wave height is estimated as follows:

$$H_S^{Swell} = \sqrt{(H_S^{Swell-1})^2 + (H_S^{Swell-2})^2}. \quad (4)$$

The advantage of this approach is that six parameters can be compared in total (H_s , T_m , T_{m1} , T_{m2} , $H_S^{Swell-1}$, $H_S^{Swell-2}$). The dispersion relation relates the wave properties wavelength, frequency, and depth, using Eq. (5):

$$w^2 = gk \tanh(kh) + U, \quad (5)$$

where g is gravitational acceleration, k is the wavenumber, $k = \frac{2\pi}{l_p}$, w_p is the angular peak frequency, and $w_p = 2\pi f_p = \frac{2\pi}{T_p}$. The water depth is necessary to estimate the Lp. U is a component of the surface currents in wave propagation direction. In this study, U term is negligible.

L_{p-DPD} is computed using DPD-NDBC measurements and dispersion equation for comparison purposes against optimized L_p.

2.3.3. Roughness length estimation

Wave steepness ($\delta = H_s/L_p$) is defined as the ratio between H_s and the L_p. In this study, to get an overview of z_0 variations, the Taylor and Yelland representation [5] has been used to compute the z_0. This representation has been derived from three different datasets from different regions, wind conditions, and water depths, using Eq. (6).

$$\frac{z_0}{H_s} = 1.2 \times 10^2 \delta^{4.5}. \quad (6)$$

The computed values of z_0 were categorized based on wind direction, distinguishing between offshore and onshore winds (see the wind rose in Fig.1). To illustrate the variation in z_0, the values were averaged and normalized for each buoy. The normalized values, ranging from 0 to 1, were used to determine z_0 at each buoy location. The mean values of H_s, L_p and z_0 were computed for each station, unless the station has fewer than 30 observations. Out of the 20 stations, 12 had more than 30 observations.

3. Results

3.1. Significant wave height and second moment wave period against NDBC reference measurement

As illustrated in Fig. 2, about 1900 SAR observations were collocated with NDBC measurements. The RMSE for H_s and period T_{m2} against the reference NDBC measurements were about 0.43 m and 0.8 sec, respectively.

3.2. Peak wavelength and period estimation

The spectral peak wave period (T_p) was estimated after optimization of JONSWAP model with six derived sea state parameters for each collocated point, as illustrated in Section (2.3.2)

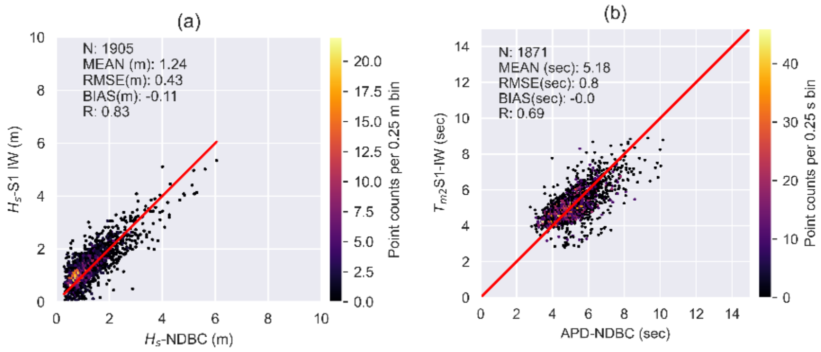

Fig.2. Validation results of the SAR collocated points with NDBC buoys: (a) H_s-S1 IW vs H_s-NDBC, (b) T_{m2}-S1 IW vs APD-NDBC

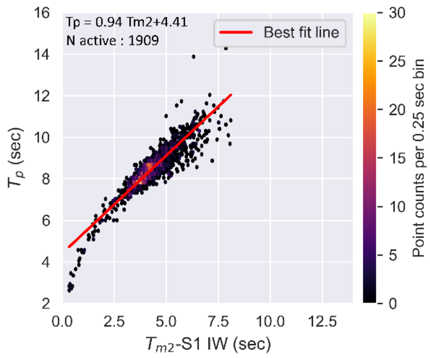

Fig.3. Spectral peak wave period ($\boldsymbol{T_p}$) correlates with second moment wave period ($\boldsymbol{T_{m2}}$) for about 1900 observations.

The estimated peak wave period (T_p) is correlated with all moment wave periods. But Fig.3 demonstrates the correlation with only T_{m2}. T_p is larger than T_{m2} with an average offset of approximately 4.5 sec. To estimate the L_p for each observation using Eq. (5), the peak wave frequency (fp) or T_p and water depth are the input parameters.

3.3. Peak wavelength, significant wave height, and normalized roughness variation (offshore wind as an example).

The impact of water depth on the retrieved wave parameters is illustrated in Fig 4. It presents the variation of the mean H_s, L_p, and normalized z_0 with respect to the water depth. Fig.4a demonstrates that the H_s from CWAVE_EX results are close to the H_s-NDBC. The comparison shows the optimized L_p is in the range of 5 m to 25 m higher than L_{p-DPD}, but the difference becomes small (< 10 m) at shallow water depths (Fig.4b). Most stations located close to the coastline at water depths less than 50 m show the highest values of normalized z_0 values (e.g., 44099, 41008, and 41013). Conversely, the far offshore stations, with water depths up to 4500 m (41001 and 41002), exhibit low normalized z_0 values (see Fig.5).

4.0 Conclusion

The validation outcomes of H_s and T_{m2} revealed the reliability of using SAR to retrieve the sea state parameters. The RMSE values were 0.43 m and 0.8 sec, respectively. The Bias were -0.11 m and 0.0 sec, respectively. The differences between L_p and L_{p-DPD} were overestimated and in range between 5 m to 25 m, slight overestimation was found in shallow waters compared with deep waters.

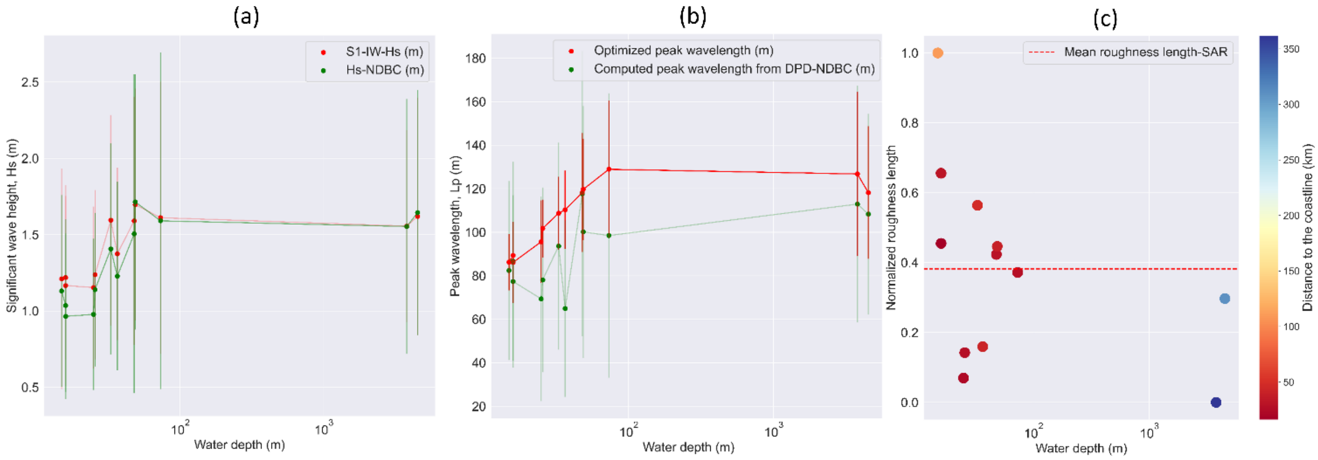

Fig.4. (a) Average H_s measurements from CWAVE_EX (red) and H_s from NDBC (green), (b) Average optimized L_p using JONSWAP and derived sea state optimization method (red) and computed L_{p-DPD} using NDBC and dispersion equation (green), (c) normalized average z_0 using Taylor and Yelland representation. Hints: the scatter points represent the NDBC stations with filter observations > 30.

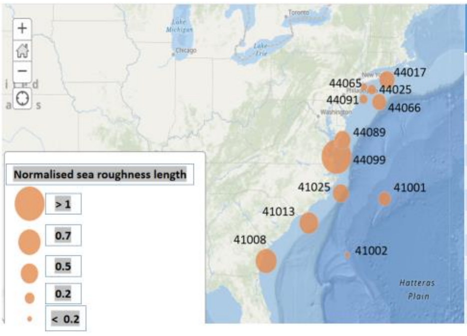

Station	Water depth (m)	Normal. Z0
44099	15	1
41008	16	0.66
41013	33	0.56
44089	16	0.45
41025	48	0.45
44017	48	0.42
44066	73	0.37
41001	4502	0.29
44025	36	0.16
44091	25.6	0.14
44065	25	0.06
41002	3784	0.0

Fig.5. Normalized mean roughness length for the 12 NDBC buoys, the table in the Figure gives information on the water depth at each station and magnitude of normalized z_0.

The results demonstrate the effects of undersea topography on the sea state. Fig 4 a and b demonstrate a reduction in H_s and L_p as the water depth decreases. These variations, along with other influencers such the distance to the coastline, lead to different magnitudes of the z_0. Most of the buoys located with water depth and distances to the coastline less than 50 m and 50 km, receptively, exhibited high normalized z_0 values. The smallest normalized z_0 values were found for the farthest offshore buoys, with distances to the coastline and water depths greater than 300 km and 3500 m, respectively. The highest magnitudes of normalized z_0 values were found for the buoys at water depth less than 36 m. However, three stations (44065, 44091 and 44025) had smaller normalized z_0 than expected even though they have shorter distance to the coastline and water depth less than 50.

5.0 ACKNOLEDGMENTS

The PhD of main author is funded by the European Union Horizon 2020 research and innovation program under grant agreement no: 861291 as part of train2wind network (https://www.train2wind.eu/). Travel support has been granted through the ESA DRAGON5 project Remote Sensing of Changing Coastal Marine Environment (ReSCCoME), ID.57192.

6.0 REFERENCES

[1] J. A. P. Veiga and M. R. Queiroz, “Impact of the Waves on the Sea Surface Roughness Length under Idealized Like-Hurricane Wind Conditions (Part II),” *Atmospheric and Climate Sciences*, vol. 05, no. 03, pp. 326–335, 2015, doi: 10.4236/acs.2015.53025.

[2] B. Jrgen, B. Lange, and S. Larsen, “Comparison Of Sea Surface Roughness Models For Offshore Wind Power Utilisation,” *EWEA special topic*, no. 1, pp. 2–5, 2001, [Online]. Available: http://www.core.org.cn/mirrors/tudelft/tudelft/ocw.tudelft.nl/fileadmin/ocw/courses/OffshoreWindFarmEnergy/res00034/Surface_roughness_paper_OWEC_2001.pdf%0Ahttp://citeseerx.ist.psu.edu/viewdoc/summary?doi=10.1.1.59.6894%0Ahttp://www.core.org.cn/mirrors/tu.

[3] Z. Gao, Q. Wang, and M. Zhou, “Wave-dependence of friction velocity, roughness length, and drag coefficient over coastal and open water surfaces by using three databases,” *Advances in Atmospheric Sciences*, vol. 26, no. 5, pp. 887–894, 2009, doi: 10.1007/s00376-009-8130-7.

[4] X. Larsén *et al.*, *Extreme winds and waves for offshore turbines: Coupling atmosphere and wave modeling for design and operation in coastal zones*, vol. 154, no. October. 2017.

[5] P. K. Taylor and M. J. Yelland, “The dependence of sea surface roughness on the height and steepness of the waves,” *Journal of Physical Oceanography*, vol. 31, no. 2, pp. 572–590, 2001, doi: 10.1175/1520-0485(2001)031<0572:TDOSSR>2.0.CO;2.

[6] A. Pleskachevsky, B. Tings, S. Wiehle, J. Imber, and S. Jacobsen, “Multiparametric sea state fields from synthetic aperture radar for maritime situational awareness,” *Remote Sensing of Environment*, vol. 280, no. September 2021, 2022, doi: 10.1016/j.rse.2022.113200.

[7] A. Pleskachevsky, S. Wiehle, S. Jacobsen, and M. Safety, “Multiparametric Sea State Fields from Synthetic Aperture Radar for Maritime Situational Awareness,” pp. 1–42, 2021.

[8] K. Hasselmann *et al.*, “Measurements of wind-wave growth and swell decay during the joint North Sea wave project (JONSWAP).,” no. July 2015, 1973.